Analysis of Sensorless Controlled Two Phase Brushless DC Motor

ABDEL-KARIM DAUD
Electrical and Computer Engineering Department
Palestine Polytechnic University (PPU)
P.O. Box 198 Hebron, Tel:+972-2-2228912, Fax:+972-2-2217248
PALESTINE

Abstract: - Using neodymium-iron-boron (Nd-Fe-B) magnets, a brushless dc motor (BLDCM) with Two air-gap windings and special form of rectangular PM-rotor is realized. Rectangular PMs are glued on the rotor in order to reduce cost. Sensorless techniques are becoming more attractive for drives, since they can result in less expensive and more robust system. Especially in BDCM drives, where the rotor position is fundamental to derive the proper switching sequences, this is a very interesting issue. Therefore, a sensorless strategy, which is based on extracting information from the back-emf, is used. The calculation of the air-gap flux density is obtained by using a 2DFEM program. Flux lines distribution in the electromagnetic parts of this motor is obtained also for different rotor position. Then the obtained results of the magnetic flux density are decomposed in harmonic spectrum by means of Fast Fourier Transforms (FFT). The motor parameters and characteristics are also determined by using FFT. Motor characteristics are calculated and measured. The measured results show good agreement with theoretical results

Key-Words: - BLDCM, permanent magnets, 2DFEM, sensorless control, FFT

1 Introduction

Permanent-magnet excited brushless dc motors (BLDCM) are becoming increasingly attractive in many applications due to their performance advantages such as reduced size and weight, high efficiency, low noise and maintenance, improved reliability and very good control characteristics in a wide speed range [4,5,7,11,12]. The interest in the brushless dc drives has also consequently increased with the development of microelectronic and power electronics [6,7].

The most popular brushless DC motors have three-phase windings [1,2] or four-phase windings [3], which are controlled and driven by full bridge transistor circuit.

From these classical types of brushless dc motor with three or four windings, it became clear that the electronic circuit is still expensive so that this type of motor could not be used in consumer applications.

In this paper, a brushless DC motor with only one air gap winding and special form of PM-rotor is investigated. For the electronic circuit only two power switches is necessary. Therefore, the cost of such a drive is reduced.

Elimination of position and velocity transducers in dc drives is desirable for a number of reasons. The shaft transducers themselves and perhaps even more the associated wiring, are a significant source of failure and cost. However, for a good performance of the PM dc motor, the rotor position has to be known with high accuracy. Much effort, reflected in the numerous papers dealing with this issue, has been made in research to avoid use of a position sensor in dc drives [8,9,10]. In this paper, the detection of back-emf technique is used.

Due to the complex arrangement of PM-rotor as shown in Fig.1, the air gap flux density is obtained by using a 2DFEM program. By using the method of FFT, the different motor parameters and characteristics are determined.

2 Drive Description

The block diagram of a two-pole, two-phase brushless dc motor drive is shown in Fig.1.
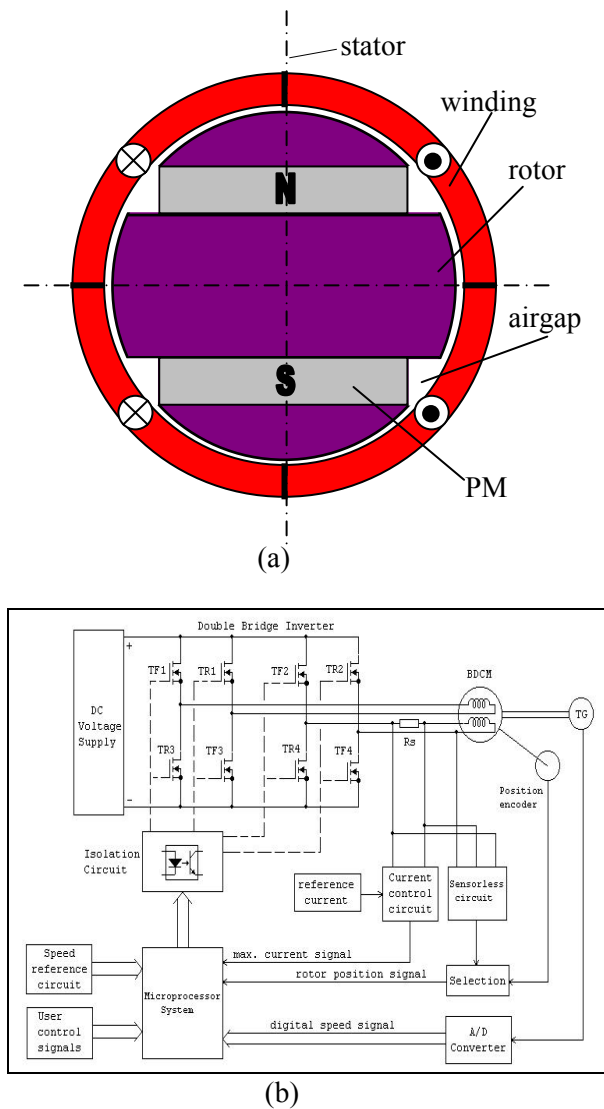
(a)

(b)

Fig.1: Internal rotor two phase brushless DC motor and drive

The overall system consists of four parts: electromagnetic structure, power converter and commutation control. The electromagnetic structure, as shown in Fig.1a, is formed by a special form of an internal rotor that has a rectangular permanent magnet arrangement in order to reduce cost, and a slotless stator assembly that consists of a lamination stack with air gap windings. The construction and distribution of stator windings are shown in Figs.2 and 3. The motor has two phases. Each phase consists of four coils. These coils combine two parallel groups. Each group consists of two series coils at the same radius as shown in Fig.2. Therefore, the first phase has the two parallel groups: (A0.0, B0.0) and (A1.0, B1.0), while the remaining coils (A0.5, B0.5) and (A1.5, B1.5) combine the second one.
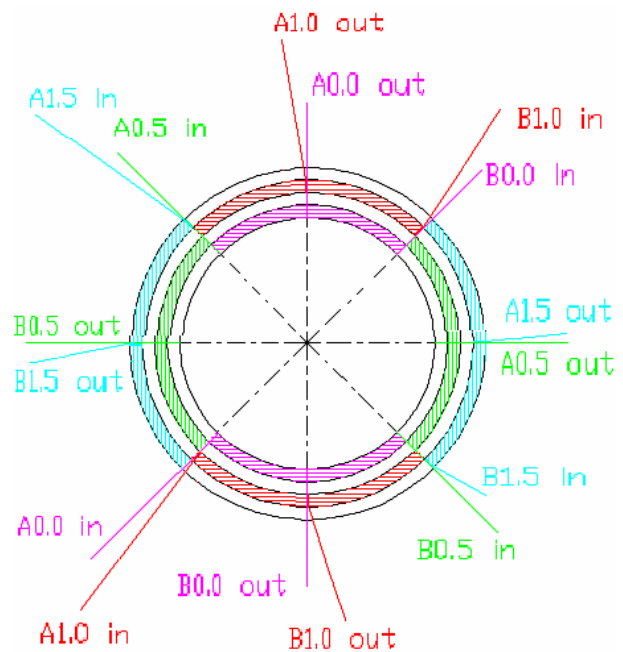

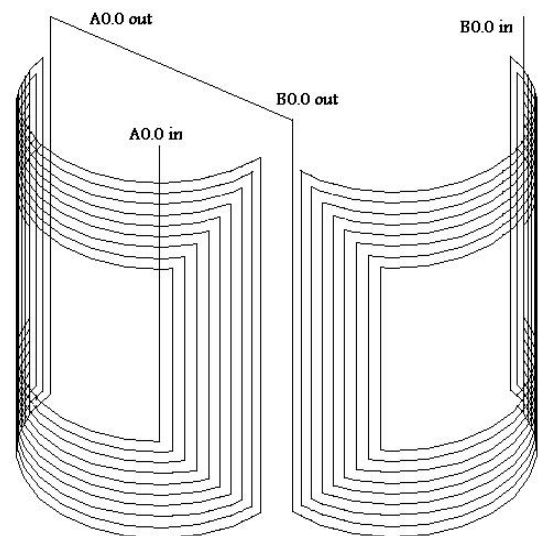Fig. 2: Construction of stator windings

Fig. 3: One group-phase connection

In this case, the current will flow in each phase for a period of about (180°) for every rotor revolution. An increase in the number of phases will only provide a slight increase in the average torque, but it requires more power switches for the electronic commutation circuit. The power converter, as shown in Fig. 1b, is a double bridge circuit (inverter) that provides the required sequence of the phase voltages in both directions. The power MOSFETs receive their gate signals from the microprocessor through the 8155 PID interface circuit. Detection of the rotor position

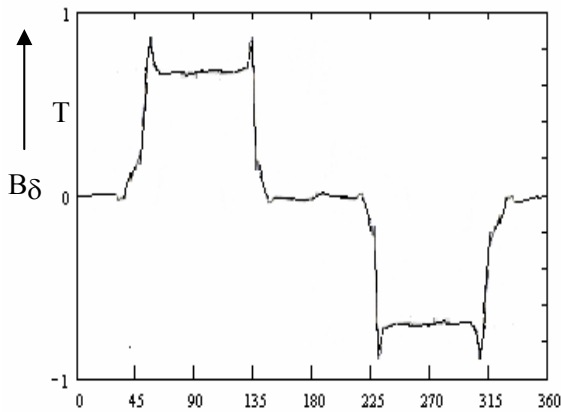can be achieved through photocell or sensorless control circuit.

Fig.4: Air gap flux density of the motor $B\delta = f(\alpha)$

2 Air Gap Flux Density

Due to the complex arrangement of PM-rotor as shown in Fig.1a, the air-gap flux density B_δ is obtained from a 2DFEM program, which distribution is illustrated in Fig.4. The Fourier series for this curve, is displayed for the harmonic $\nu=12$ in Fig.5. It is clear, by increasing the number of Fourier coefficient, the flux density $B_\delta = f(\alpha)$ comes closely to the origin function. Theoretically when $\nu = \infty$, man obtained exactly the original function.

3 System Model

Fig. 6 shows the equivalent circuit for one winding. The angle α in Fig.6 will give the actual position of the rotor. During $\alpha_1 \leq \alpha \leq \alpha_2$ the winding is energized from the dc source with the voltage V, in which the induced voltage is positive as shown in Fig.7. Therefore, the transistor switches on this period, which is called a current flow angle δo and given by

$$\delta o = \alpha_2 - \alpha_1 \qquad (1)$$

where α_1 and α_2 are switch-on and -off angles respectively. For the electronic switch a voltage drop of V_T is assumed. The curve of transistor voltage V_T is represented in Fig.8.
By inspection of Fig.7:

$$V = e + R\,i + L\frac{di}{dt} + V_T \quad \text{for } \alpha_1 \leq \alpha \leq \alpha_2 \qquad (2)$$
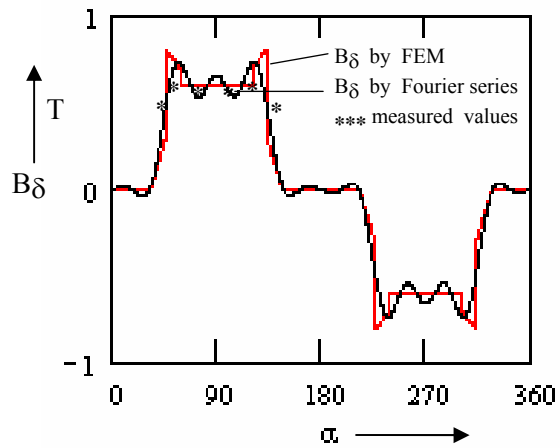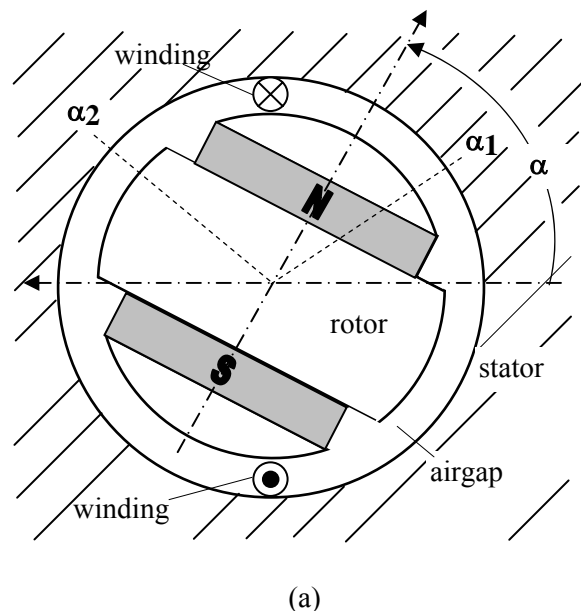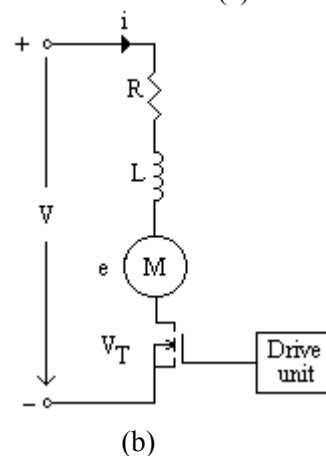

Fig.5: Fourier representation with $\nu=12$ and the original function of B_δ comparing with measured values

(a)

(b)

Fig.6: Drive circuit configuration of the motor
With

$$\alpha = \omega\, t \quad \text{and} \quad \frac{d}{dt} = \omega \frac{d}{d\alpha} \quad , \tag{3}$$

the governing equation can be arranged into the following form:

$$Ri(\alpha) + \omega L \frac{di}{d\alpha} = V - e(\alpha) - V_T(\alpha) \quad \text{for } \alpha_1 \le \alpha \le \alpha_2 \tag{4}$$
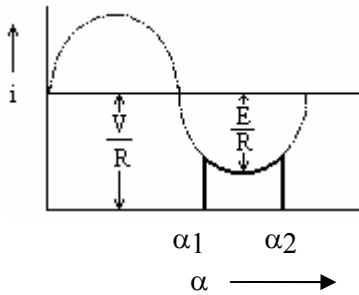

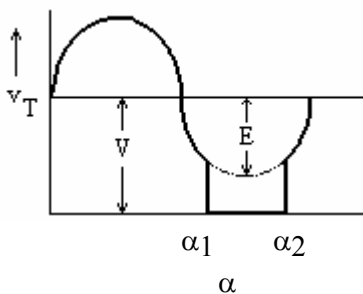Fig.7: Phase current as function of rotor position for $L \;\; 0$

Fig.8: Transistor voltage as function of rotor position for $L \;\; 0$
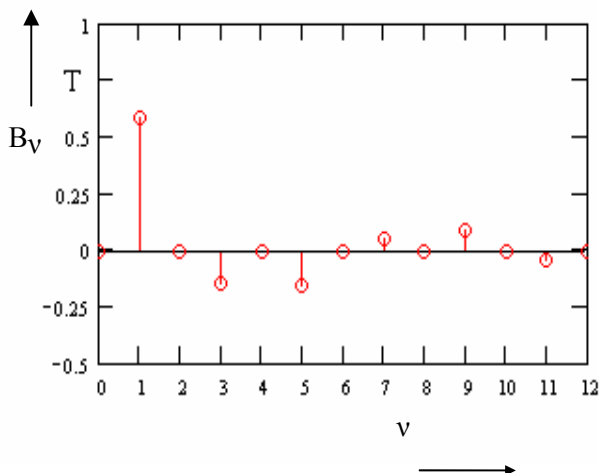

Fig.9: Harmonic spectrum of the flux density in the air gap B_v

5 Voltages and Currents

The harmonic spectrum of the magnetic flux density in Fig.5 can be obtained by applying the method of FFT, which results are shown in Fig.9. Each winding is characterized by number of windings, average diameter of winding, active length and winding parameter.

Therefore the induced voltages can be written as

$$e = \sum_{v \;\; odd} E_v \sin[v\,\alpha] \tag{5}$$

where

$$E_v = C_m\, \omega\, B_v \tag{6}$$

where C_m is the motor constant.

For steady state conditions, for $L = 0$ and assuming that the power switch is to be ideal, the solution of eq.(4) is given by:

$$i(\alpha) = I_0 + \sum_{v \;\; odd} I_v \sin(v\alpha) \tag{7}$$

where

$$I_0 = (V/R) \quad \text{and} \quad I_v = E_v / R ; \tag{8}$$

The average value of the armature current can be calculated over the period $(0, 2\pi)$ and is given by:

$$I_{ave} = \frac{1}{2\pi} \int_o^{2\pi} \sum_{j=1}^{N} i_j(\alpha) d\alpha \tag{9}$$

where N is the number of armature phases.

For additional calculations, the average current is given by

$$I_{ave} = \frac{N}{2\pi} [\, I_0\, \delta o + \sum_{v \;\; odd} I_v\, a_1/v\,] \tag{10}$$

where

$$a_1 = 2 \sin(v\beta) \sin\delta o \quad \text{and}$$
$$\beta = \pi - (\alpha_2 + \alpha_1) \tag{11}$$

6 Torque

The gross electromagnetic torque is given by /7/:

$$T = C_m\, B_v\, i \sin(v\alpha) \tag{12}$$

Taking into account eqs. (7) and (12), the instantaneous torque of the motor is

$$T = \frac{1}{\omega R} \left\{ \sum_{v \ odd} V E_v \sin(v\alpha) + \sum_{v \ odd} E_v^2 \sin^2(v\alpha) \right\} \quad (13)$$

In order to produce a continuous torque, two or more phases have to be energized in sequence. Therefore, the average torque can be calculated over the period $(0 , 2\pi)$ during the current flow angle δo.

$$T_{ave} = \frac{N C_m V}{2\pi R} \sum_{v \ odd} \frac{B_v a_1}{v} +$$

$$- \frac{N C_m^2}{4\pi R} \left(\sum_{v \ odd} B_v^2 \ a_2 \right) \omega \quad (14)$$

where

$$a_2 = \delta o - \sin(v\delta o) \cos(2v\beta) \quad (15)$$

For additional calculations, the following equations for the torque and voltage are obtained:

$$T_{ave} = \frac{C_m}{\delta o} \sum_{v \ odd} \frac{B_v a_1}{v} \ I_{ave} +$$

$$- \frac{N C_m^2}{4\pi R \delta o} \left[\sum_{v \ odd} B_v^2 (v^2 \delta o \ a_2 - 2 a_1) \right] \omega \quad (16)$$

$$V = \frac{C_m}{\delta o} \left(\sum_{v \ odd} \frac{B_v a_1}{v} \right) \omega + \frac{2\pi R}{\delta o \ N} \ I_{ave} \quad (17)$$

7 Results

The previous described method has been applied to a two pole, two phase brushless DC motor with air gap windings. The main design parameters are given in Table 1. The special feature of this brushless DC motor is, that no rotor position sensors, such as Hall probes or magnetoresistive sensors, are used. For detection of rotor position the induced voltage is used in combination with an electronic circuit.

A 2D- finite element program was used for field calculations. Fig.5 shows the simulated and measured values of the air gap flux density. The magnetic flux distribution in the electromagnetic parts of the motor for different rotor position and armature current as obtained on the basis of the FEM is shown in Figs. 10 and 11. From Fig.11, it is clear due to air gap winding, the influence of the armature

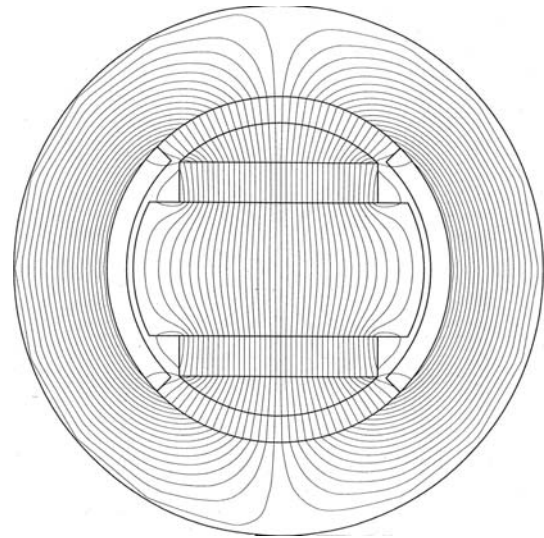field on the main field is very low. Therefore, the armature reaction can be neglected.

Fig.10: Magnetic flux distribution for I=0A and $\alpha=0°$.
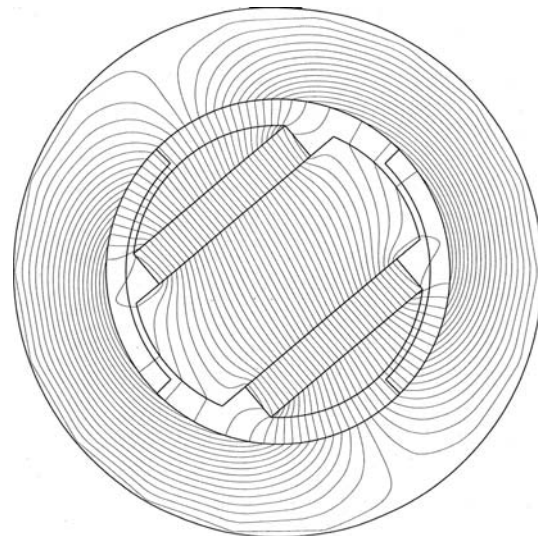

Fig.11: Magnetic flux distribution for I=4A and $\alpha=220°$ for one phase.

The instantaneous phase current is shown in Figs.12 and 13 for different speeds. For different supply voltages V, the calculated and measured speed – torque characteristics of the motor are represented in Figs.14. The linear speed - torque shows that by the variation of the applied voltage, very wide ranges may be obtained. Current versus torque is given in Fig.15 for different speeds. The

calculation results are in good agreement with test results.

8 Conclusions

A brushless DC motor with two phases is described in this paper. This motor type has air gap windings and special form of Nd-Fe-B PM-rotor. By applying the method of Fast Fourier transforms (FFT); the calculated results of the magnetic flux density obtained on the basis of the FEM are decomposed in harmonic spectrum. The influence of current harmonics is studied. Motor characteristics are measured and calculated. The measured results show good agreement with the theoretical results.

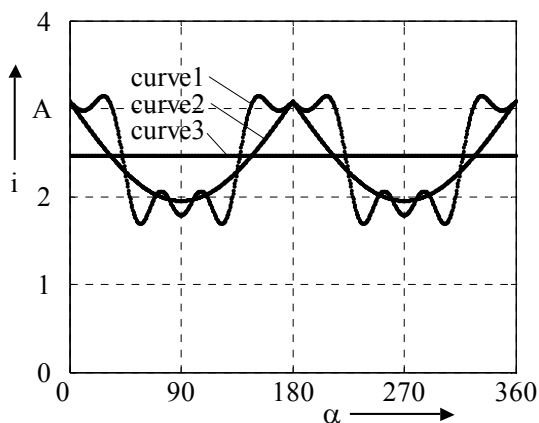| Item	Dimension
no. of phases	N = 2
current flow angle	δo = 180°
no. of windings	62
angle of the winding	90°
winding resistance	R = 1.3 Ω
self-inductance	L = 35mH
pole number	2p=2
PM:	
length	30 mm
width	30 mm
height	6 mm
material	NdFeB

Table 1: Design data of BLDCM

Fig.12: Phase current of the motor at n=1000 rpm and L = 0.
curve 1: calculated using five Fourier coefficient
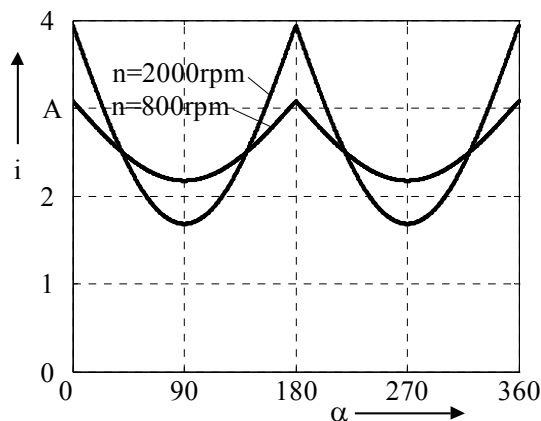curve 2: calculated using one Fourier coefficient
curve 3: average value

Fig.13: Instantaneous current of the motor for L=0 and the same average value (I_{ave} = 2.5A).
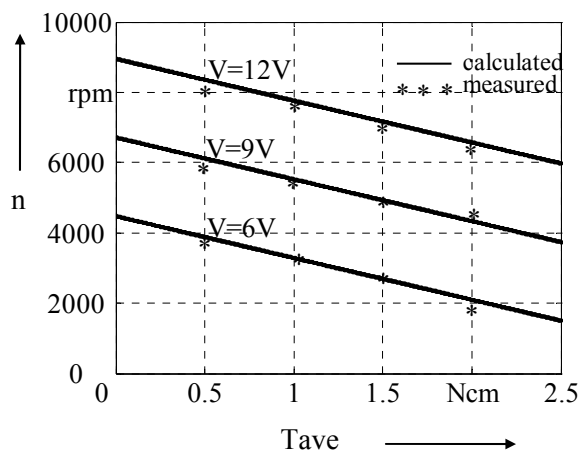

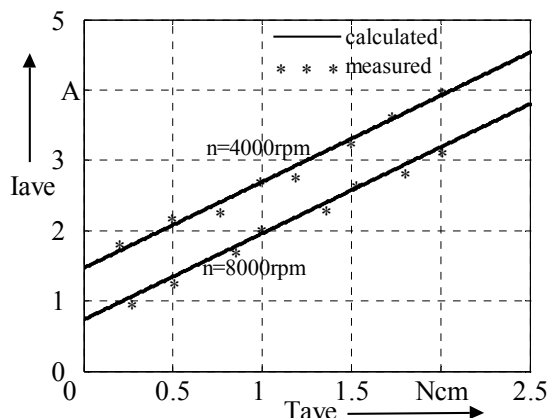Fig.14: Speed / torque characteristics with the voltage supply V as parameter

Fig.15: Current / torque characteristics with the motor speed n as parameter

References:

[1] B. Ackermann; E. Bolte; D. Howe; M.K. Jenkins; Z.Q. Zhu, Frequency domain analysis of brushless DC motor performance, *ETEP*, vol. 2, No. 6, 1992,pp. 389-396

[2] A.-K. Daud; S.H. Khader, An analytical method for determination of commutation leading angle in three- phase brushless DC motor, *Proc. Of ELECTROMOTION'97*, Cluj-Napoca, pp. 253-258.

[3] R. Hanitsch, Analog computer simulation of brushless DC motors, *Proc. of ICEM*, 1984, Lausanne, pp. 189-192.

[4] J.M.D. Coey, *Rare-Earth Iron Permanent Magnets*, Oxford Science Publications, Clarendon Press Oxford, 1996.

[5] R. Hanitsch, Design and performances of electro-magnetic machines based on NdFeB magnets, *Journal of Magnetism and Magnetic Materials 101*, (1991) pp. 271-275.

[6] M.H. Rashid, *Power Electronics, Circuits, Devices and Applications*, Pearson Prentice Hall, Upper Saddle River, New Jersy, 2004.

[7] H.B. Ertan; M.Y. Üctung; R. Colyer; A. Consoli, *Modern Electrical Drives*, Kluwer Academic Publishers, Netherlands, 2000.

[8] R. Wu; G.R. Slemon, A permanent magnet motor drive without a shaft sensor, *IEEE Trans. Ind. Appl.*, Vol 27, No. 2. 1991, pp. 1005-1011.

[9] L. Harnefors; P. Taube; H.-P. Nee, An improved method for sensorless adaptive control of permanent-magnet synchronous motors, *Proc. Eur. Conf. Power Electronics*, Trondheim, Vol 4, 1997.

[10] N. Matsui, Sensorless permanent-magnet brushless DC and synchronous motor drives, *ELECROMOTION*, Vol 3, No. 4, 1996, pp. 172-180.

[11] J.D. Ede; Z.Q. Zhu; D. Howe, Design considerations for high-speed permanent magnet brushless dc motors, *Proc. International Conference on Power Electronics, Machines, and Drives, IEE*, 2004, pp. 686-690.

[12] B.-K. Lee; M. Ehsani, Advanced simulation model for brushless dc motor drives, *Electric Power Components and Systems*, September 2003, pp 841-868.